The Calculations of Dispersion Coefficients Inside Two-dimensional Randomly Packed Beds of Circular Particles

Amir Jourak, Vilnis Frishfelds, and T. Staffan Lundström
Division of Fluid and Experimental Mechanics, Luleå University of Technology, SE-971 87, Luleå, Sweden

Inga Herrmann and Annelie Hedström
Dept. of Civil, Environmental and Natural Resources Engineering, Luleå University of Technology, SE-971 87, Luleå, Sweden

DOI 10.1002/aic.13867
Published online July 17, 2012 in Wiley Online Library (wileyonlinelibrary.com).

The longitudinal (D_L) and transverse (D_T) dispersion coefficients in two-dimensional (2-D) randomly packed beds of circular particles in a laminar flow regime are derived. A 2-D discrete system of particles is divided into cells using modified Voronoi diagrams. The relationship between the variation of the stream function and the averaged vorticity is obtained from computational fluid dynamics (CFD) simulations. The whole flow pattern is then obtained by using the principle of energy dissipation rate minimization. The obtained values of D_L agree well with 3-D experimental data for all velocities investigated. At very high velocities, D_T in 2-D appears to be higher than 3-D experimental data. In addition, the effects of particle-size distributions, packing structure, and porosity on the D_L and D_T were studied. One result was that an increase in the width of the particle-size distribution resulted in higher values of D_L and D_T at high velocities. © 2012 American Institute of Chemical Engineers *AIChE J,* 59: 1002–1011, 2013
Keywords: longitudinal dispersion, transverse dispersion, dispersion, packed beds, mass transfer

Introduction

The study of dispersion in flow through porous media is a significant issue in many branches of science and engineering, and has direct applications in several industries. For example, dispersion may be a central mechanism in the miscible displacement of oil and gas, the disposal of sewage waste into aquifers, and for flow through reactive compact-bed filters that are used for on-site sanitation systems. In the refining industry, the hydrodynamic dispersion properties inside packed-bed reactors are of utmost importance to control adsorption efficiency during the purification and separation processes of chemical species by an adsorption removal mechanism. Another significant application is the impregnation of fabrics during composites manufacturing. In this case, the flow is often on several scales and different kinds of particles may be added to the fluid.[1–5] Papermaking is yet another area of application as well as the manufacturing of new biocomposites where wicking may play a significant role.[6–9]

Ever since the experiments of Slichter[10] and the early studies of Taylor[11] and Aris,[12,13] this topic has been widely studied in both experimental and numerical contexts, and many books have addressed it (e.g., Bear,[14] Scheidegger,[15] Dullien[16]). A large number of theories based on probabilistic approaches have been used to describe dispersion in porous media, including the theory of Saffman,[17,18] who modeled a porous medium as a random network of capillaries, and Koch and Brady.[19] Experimental measurements of longitudinal (D_L) and transverse (D_T) dispersion coefficients are normally conducted separately. In order to measure D_L, packed-bed column experiments are usually performed with an inert tracer. Depending on the adopted boundary conditions, and by neglecting transverse dispersion, an effluent curve is fitted with available analytical solutions (for an overview see, van Genuchten and Alves[20]) to the following 1-D advection-dispersion equation

$$\frac{\partial c}{\partial t} + u\frac{\partial c}{\partial x} = D_L\frac{\partial^2 c}{\partial x^2}, \tag{1}$$

where c is the mean solute concentration, t is time, x is the distance in the main flow direction, u is the average interstitial liquid velocity, which is defined as $u = U/\varepsilon$, where U is the superficial liquid velocity, and ε is the bed voidage. The measurement of transverse dispersion is normally more difficult than the measurement of longitudinal dispersion.[15] Generally, the methods that are used to estimate D_T are based on either tracer tests or dissolution tests. For instance, the methods that have been used to measure transverse dispersion in laboratory columns include the continuous point source and the instantaneous finite source methods.[21] These methods consist of injecting a nonreactive tracer from an injector that has been embedded into a porous medium followed by concentration variation monitoring at several points that are downstream of the injection point. Another method of D_T determination, developed by Coelho and Guedes de Carvalho,[22] is based on the measurement of mass transfer rates

Correspondence concerning this article should be addressed to A. Jourak at amir.jourak@ltu.se.

between flat or cylindrical surfaces that have been buried in a bed of inert particles and the flow flowing along it. The results from such experiments, with different solutes and temperature conditions, are typically plotted as either D_L/D_m (or D_T/D_m) vs. Pe_m ($= ud/D_m$), or as Pe_L ($= ud/D_L$) or Pe_T ($= ud/D_T$) vs. Pe_m with the corresponding Schmidt numbers ($Sc = \mu/\rho D_m$). In these expressions, D_m is the molecular diffusion coefficient, d is the inert particle diameter, and ρ is density of the liquid. Such curves can be used to find correlation functions as outlined in Delgado.[23] When available in the literature, these validated correlations are used to estimate the dispersion coefficients inside packed-bed columns.

Hydrodynamic dispersion in a porous medium can also be investigated and predicted with numerical simulations. In fact, using validated numerical simulation methods is advantageous because they can provide significant time savings. Moreover, one can access and study transport properties (i.e., hydrodynamic dispersions) in the porous medium at the pore scale, which is neither easily measurable nor feasible using experimental methods. The dispersion of solute during flow in porous media is a macroscopic phenomenon dominated by pore-scale effects.[24] One numerical method to determine hydrodynamic dispersion inside packed beds of spherical particles is by means of computational fluid dynamic (CFD) simulation.[25–28] One main problem with this approach is that simulations of large systems of particles become very time-consuming. In addition, it is difficult to discretize the contact point between the particles; hence, it is often essential to contract the particle diameters so as to allow CFD calculations.[25] This particle contraction process increases the porosity of the packed-bed model and directly affects the dispersion parameters. Another issue is related to the meshing around the particles in the packed-bed model, that is, the suitability of the mesh must be analyzed in order to estimate the precision of the calculated mass-transport parameters.

This article examines detailed simulations of mass transport in 2-D packed-bed models in a laminar flow regime. The porous medium in focus consists of a discrete system of thousands of particles that are randomly packed in a 2-D domain. Modified Voronoi diagrams are used to divide the system of particles into cells that each contains one particle. The flow pattern inside of the porous medium is obtained by minimization of the energy dissipation rate.[29] A similar discrete model of a bed of particles was used to model the drying of a bed of iron ore pellets,[30] and to study filtration mechanisms during composites manufacturing,[31] as well as internal erosion processes.[32] In this study, the boundary conditions of the 2-D domain were adapted in order to perform longitudinal dispersion numerical simulations so as to calculate D_L. To study D_L for each position and time along the packed-bed model, concentration profiles were fitted with the appropriate analytical solutions in order to enable dynamic numerical simulations. By introducing other boundary conditions to the 2-D domain, a method similar to that developed by Coelho and Guedes de Carvalho[22] was used to study D_T. The results from these 2-D numerical simulations are presented as Pe_L and Pe_T vs. Pe_m, and are further compared to 2-D theoretical and 3-D experimental results. Moreover, few investigations have been performed on the effects of particle-size distributions,[33–38] packing structure, and porosity[39] on the dispersion coefficients; therefore, it is of interest to scrutinize how they influence the dispersion coefficients.

Numerical

Discrete model of a bed of particles

The consideration of a porous medium as a discrete system of particles facilitates the study of the statistical variation of the macroscopic mass-transfer coefficient that is caused by microscopic stochasticity. Such variation may originate from the size and shape distributions of the particles and their positions; however, in this case, the shape is always circular, whereas the sizes and positions are allowed to vary. In addition, the methodology proposed herein makes it possible to include the natural dispersion of an inert solute in a liquid through the porous medium. Particles can come into contact with each other, which leads to an absence of mass transport between these particles. Nevertheless, there is no need to particularly include this case, as an infinitesimal distance between particles leads to an infinitesimal mass transport through the gaps between them.

The system must be randomized in a proper way, since any systematic inhomogeneity may lead to that the concentration front travelling at different speeds and an amplification of the longitudinal dispersion in a long system (see, e.g., Huang et al.[40]). This is not the case of this random system with periodic boundary conditions, and the obtained dispersivity should be referred as the bulk dispersivity for a system with limited structural variety.

Voronoi discretization of the system

Using Voronoi diagrams, the system of particles is divided into cells that each contains one particle. Since the particles can have different sizes, a modified version of the Voronoi discretization process is used such that the Voronoi lines do not cross the surfaces of the particles.[29] The closest Voronoi lines (with respect to the surfaces of the particles) are placed in the middle of the two nearest surfaces of the particles and are perpendicular to the lines that connect the centers of the particles (see Figure 1b).

Derivation of the stream function

The particles are assumed to be impermeable, and liquid is assumed to percolate around the particles as it moves through the bed. Therefore, the stream function is constant along the surface of any given particle. No-slip boundary conditions further limit any potential variation of the stream function. The vorticity distribution results from the distribution of the stream function. For that reason, CFD results are used for the nearest three particle configurations.[29] This results in nondimensional coefficients that relate the average vorticity to the difference in the stream function within a local area. Such an approach is justified by the fact that the vorticity is always highest at or at least near to the closest spacing between two neighboring particles, as estimated by the analytical formulas in Lundström and Gebart[41] and the CFD calculations in Hellström et al.[42] for periodic systems. For low Reynolds number (Re), the energy dissipation rate can be minimized according to the following equation

$$\int \mu\omega^2 dV = \min, \tag{2}$$

where ω is the vorticity that was used to obtain the distribution of the stream function.[29,43] This is, for instance, true for laminar flow as in reactive compact-bed filters. Because the energy dissipation rate quadratically depends on vorticity, a

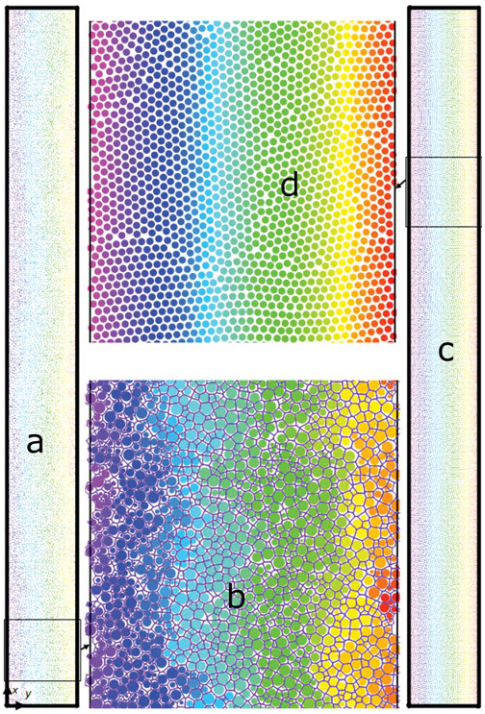

Figure 1. Examples of 2-D systems with dimensions 5.0 × 0.5 m² that consist of about 15,000 particles.

The color represents the value of the stream function for each particle, (a) simulation F, (b) part of Figure 1a showing the Voronoi mesh, (c) simulation D, and (d) part of Figure 1c showing the packing structure in simulation D. [Color figure can be viewed in the online issue, which is available at wileyonlinelibrary.com.]

linear system of equations with respect to the stream function values for the particles can be found, and the velocity distribution can be computed as illustrated in Figure 1.

Molecular diffusion

The application of Voronoi diagrams facilitates the calculation of molecular diffusion in the space between particles. Thus, the complete mass transport, taking into account the detailed flow patterns in the system, can be derived. The liquid flows along the Voronoi lines in the system, and the same is true for diffusion. Each Voronoi line segment has two neighboring Voronoi lines at one end point, and two Voronoi lines at the other end point. The result is a channel-like network of heat and mass transport where each channel is represented by one Voronoi line. The smallest width of the channel is at the location between two neighboring particles, whereas the width of the channel is wider at the connection points of three Voronoi lines. This makes it possible to build a network model where each node is placed at a connection point of three Voronoi lines. Each channel that connects neighboring nodes must have a proper heat and mass resistance. The effective width-to-length ratio of the channel δ_{eff}, is calculated in such a way that it has the same mass transport properties as a real channel between two round particles. It can be found by the same approach as in Lundström and Gebart[41] when deriving the transverse permeability of fiber bundles. In this case δ_{eff} is defined by an integral according to

$$\frac{1}{\delta_{eff}} = \int_{x_1}^{x_2} \frac{1}{d_0 + r_1 - \sqrt{r_1^2 - x^2} + r_2 - \sqrt{r_2^2 - x^2}} dx \approx \sqrt{\frac{2r_1r_2}{d_0(r_1+r_2)}} \arctan\left[\sqrt{\frac{r_1+r_2}{2d_0r_1r_2}}x\right]\Bigg|_{x_1}^{x_2}, \quad (3)$$

where the integral is taken over the actual spacing between particles along one Voronoi line with length $l = x_2 - x_1$ assuming that the smallest distance between the particles d_0 at $x = 0$ is much smaller than the radius of particles r_1 and r_2. This is valid if the porosity of the system is low or the system is well packed. Equation 3 can be further simplified by assuming that arctangent for a small d_0 and a long Voronoi line is unity, yielding the following expression

$$\frac{1}{\delta_{eff}} \approx \pi\sqrt{\frac{2r_1r_2}{d_0(r_1+r_2)}}. \quad (4)$$

As can be seen, the result does not depend on the length of the channel, which is a consequence of all the resistance to mass and heat transport stem from the space where the distance between particles is smallest with the assumptions introduced. The discretized mass-transport equation becomes

$$V_k\frac{\partial c_k}{\partial t} + v_{0k1}d_{0k1}c_{0k1} + v_{0k2}d_{0k2}c_{0k2} + v_{0k3}d_{0k3}c_{0k3} = D_m\left(\delta_{eff\,k1}\frac{c_{k1}-c_k}{l_{k1}} + \delta_{eff\,k2}\frac{c_{k2}-c_k}{l_{k2}} + \delta_{eff\,k3}\frac{c_{k3}-c_k}{l_{k3}}\right), \quad (5)$$

where V_k is the volume of the cell; $k1$, $k2$, $k3$— indices for neighboring cells in the space between particles; $0k1$, $0k2$, $0k3$— indices for the position toward neighboring cells at the smallest spacing; v is the velocity component going outwards at the corresponding spacing. Since the flow rate is slow in spaces between closely packed particles, the mass transfer rate at these locations is low. The discrete numerical schemes for the advection-diffusion equation may have numerical instability. Therefore, a corrected upwind numerical scheme is used. This choice may slightly increase the apparent diffusion for very high flow rates; however, the approach is valid when the discretization Peclet number ($\mathrm{Pe_{dis}} = ud_{dis}/D_m$, where d_{dis} is the size of discrete element) is small (i.e., $\mathrm{Pe_{dis}} < 1$). Since the size of an element is comparable with the particle diameter, $\mathrm{Pe_m} = 200$ is used as the uppermost limit where the numerical scheme remains accurate for the purposes of the study, i.e., dispersion in flow through a packed bed in a laminar flow regime. Herein, only molecular diffusion is assumed as diffusion mechanism and the effect of turbulence is neglected. This is valid if Re with respect to the particle diameter remains small (i.e., $\mathrm{Re} < 100$ [42]) or Sc at any given $\mathrm{Pe_m}$ remains large (i.e., $\mathrm{Sc} \gg 1$). Additional dispersion associated with parabolic velocity profiles in the narrow gaps is important only at $\mathrm{Pe_m} \gg 1$ and can be neglected for the given range of velocities.

Longitudinal dispersion

In order to calculate D_L, a rectangular 2-D planar system consisting of a random distribution of particles is studied. The main flow is directed upward, and on the lower side a constant concentration c_0 is applied, whereas on the upper side, there is no diffusional flux. The side walls have periodic boundary conditions. Because of the random distribution of

particles, there is a slight variation in concentration in the direction that is perpendicular to the main flow direction. Therefore, the concentration is averaged in the perpendicular direction in order to obtain the 1-D profile of the flow front. The averaged concentration is calculated as volume-averaged concentration $= \int_0^a \int_{x-\Delta/2}^{x+\Delta/2} c dx dy/(a\Delta)$, and flow-averaged concentration $= \int_0^a u_x c dy / \int_0^a u_x dy$, where a is the width of the 2-D packed bed, Δ is the thickness of the thin layer for the volume averaging, and u_x is the velocity component in the x-direction of the discrete 2-D domain. This is then compared to the analytical results for the 1-D advection-diffusion equation.

The corresponding 1-D advection-diffusion problem is set by Eq. 1, and the following boundary conditions

$$\begin{aligned} &c = 0, \quad 0 < x \le L, \quad t = 0, \\ &c = c_0, \quad x = 0, \quad t \ge 0, \\ &\frac{\partial c}{\partial x} = 0, \quad x = L, \quad t \ge 0. \end{aligned} \tag{6}$$

This setup has the following approximate analytical solution[20]

$$\begin{aligned} \frac{c}{c_0} = &\frac{1}{2}\mathrm{erfc}\left(\frac{x-ut}{2\sqrt{D_L t}}\right) + \frac{1}{2}\exp\left(\frac{ux}{D_L}\right)\mathrm{erfc}\left(\frac{x+ut}{2\sqrt{D_L t}}\right) \\ &+ \frac{1}{2}\left[2 + \frac{u(2L-x)}{D_L} + \frac{u^2 t}{D_L}\right]\exp\left(\frac{uL}{D_L}\right)\mathrm{erfc}\left(\frac{2L-x+ut}{2\sqrt{D_L t}}\right) \\ &- \sqrt{\frac{u^2 t}{\pi D_L}}\exp\left[\frac{uL}{D_L} - \frac{(2L-x+ut)^2}{4D_L t}\right]. \end{aligned} \tag{7}$$

The exact solution of Eq. 1 when using the boundary conditions (Eq. 6) is in the form of an infinite series. Equation 7 will provide an accuracy of at least four significant digits when either of the following conditions are satisfied[20]

$$\frac{uL}{D_L} > 5 + 40\frac{ut}{L}, \text{ or } \frac{uL}{D_L} > 100, \tag{8}$$

where $\mathrm{Pe_c} = uL/D_L$ is a column Peclet number. In the numerical simulations here presented, only at very low $\mathrm{Pe_m}$, i.e., $\mathrm{Pe_m} < 0.2$, the aforementioned conditions are not satisfied; however, the approximate solution, Eq. 7, and the exact solution (via the CFITM code[44]) are used to fit the effluent curves that are obtained from the model as an example for one numerical simulation at low $\mathrm{Pe_m}$. The difference between the approaches will, therefore, be scrutinized.

The D_L that is used to calculate $\mathrm{Pe_L}$ was obtained by comparing the numerical result to the analytical solution of the 1-D problem, Eq. 7, for a fixed u. This can be achieved by either fitting the analytical solution to the concentration profile as a function of x at a fixed time t, or by fitting the analytical solution to the concentration profile as a function of t for a fixed coordinate x. The fitting is done using Newton's optimization technique in combination with the least-squares method. In order to achieve such a fitting, the first and second derivatives of the analytical solution must be known. The initial guess of D_L must be in the vicinity of the exact value in order to establish a correct fitting.

In the numerical simulation, a fixed U and ε were imposed on the setup. Therefore, a fixed u for the estimation of D_L (as described earlier) was used. Another approach that is often applied in packed-bed column experiments is to simultaneously fit both u and D_L to the measured breakthrough curve. One reason for this is that the measured ε before experiments might slightly differ from that in the packed bed during the experiments. For instance, consider the case that the large pores in the packed bed are clogged by small particles during the experiment, which can cause variation in the ε. Moreover, the material that is used in the packed-bed column experiment can be heterogeneous, which can lead to variations in u along the bed (see comparison between effective pore-water velocities in homogeneous and heterogeneous column experiments in Huang et al.[40]). In the current numerical setup, however, there is a homogeneous porous-medium model, and the particles are not allowed to move during the numerical simulation; hence, ε and u are constant during the numerical simulations.

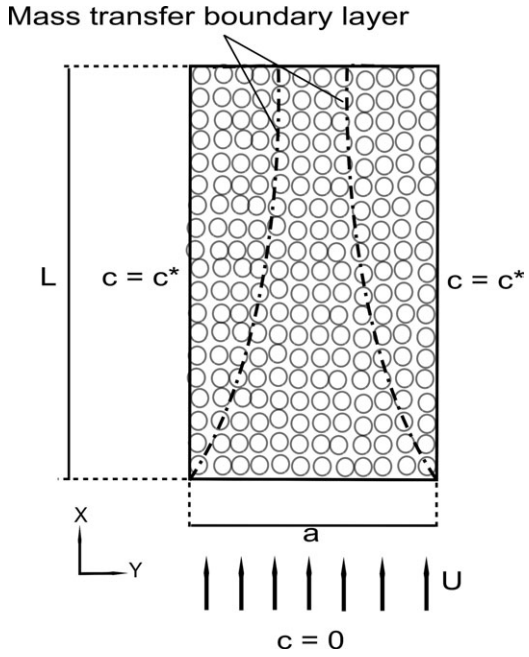

Figure 2. Schematic representation of the transverse dispersion numerical simulation setup.

Transverse dispersion

In order to calculate D_T in planar 2-D systems, a similar method to that developed by Coelho and Guedes de Carvalho[22] was applied.

The model consists of a 2-D planar packed bed with uniform ε through which the liquid flows at a superficial velocity of U (see Figure 2). The inlet concentration is set to zero, whereas the concentration of the side walls is fixed to a certain value c^*. Due to natural transverse dispersion, a mass-transfer boundary layer will develop across which the solute concentration will drop from $c = c^*$, at $y = 0$, to $c \to 0$ at the opposite side of the boundary layer. By defining a small control volume inside this boundary layer, a steady-state concentration balance can be defined as follows[22]

$$u\frac{\partial c}{\partial x} - D_T\frac{\partial^2 c}{\partial y^2} - D_L\frac{\partial^2 c}{\partial x^2} = 0. \tag{9}$$

There is no simple analytical solution for this planar problem; however, if D_L is neglected, then the solution is easily

Table 1. Characteristics of Setups used for the Longitudinal Dispersion Simulations

Case	ε	Particle diameter [mm]	System size [m^2]	τ	D_L/D_m at $Pe_m = 0.02$	D_L/D_m at $Pe_m = 0.2$	D_L/D_m at $Pe_m = 2.0$	D_L/D_m at $Pe_m = 20$
A	0.30	12	5.0 × 0.5	1.47	0.68	0.78	2.98	33.6
B1–4	0.35	12	5.0 × 0.5	1.39	0.715 ± 0.006	0.83 ± 0.01	3.00 ± 0.08	34.0 ± 0.3
C	0.40	12	5.0 × 0.5	1.37	0.73	0.85	2.90	36.0
D*	0.35	12	5.0 × 0.5	1.15	0.87	0.92	1.38	8.06
E	0.35	8–16	5.0 × 0.5	1.40	0.69	0.84	3.23	38.0
F	0.35	4–20	5.0 × 0.5	1.40	0.69	0.83	3.45	44.0
G	0.25	8–16	5.0 × 0.5	1.61	0.62	0.73	3.18	39.80
H1–4	0.35	8–16	2.5 × 1.0	1.43	0.70 ± 0.01	0.81 ± 0.01	3.10 ± 0.2	37.0 ± 2.0

*Packing is piecewise regular as in polycrystalline.
The D_L/D_m values are nondimensional longitudinal dispersion coefficients obtained from the effluent curves. The values behind "±" are standard deviations. Cases marked with 1–4 consist of four simulations with the same setup but with different random positions of particles in the system. ε is the porosity and τ is the tortuosity factor.

obtainable. This can be done if $L/d > 10$ [22], a criterion that is fulfilled in this numerical simulations since $L/d > 41$.

Thus, the setup of the problem in the system $0 \le x \le L$, $0 \le y \le a$ neglecting D_L is

$$u\frac{\partial c}{\partial x} = D_T\frac{\partial^2 c}{\partial y^2}, \tag{10}$$

$$\begin{aligned} &c = 0, \quad 0 \le x \le L, \quad 0 < y < a, \quad t = 0,\\ &c = 0, \quad x = 0, \quad 0 < y < a, \quad t \ge 0,\\ &c = c^*, \quad 0 \le x \le L, \quad y = 0 \cup y = a, \quad t \ge 0, \end{aligned} \tag{11}$$

for which an analytical solution for constant u and D_T can be derived as follows

$$\frac{c}{c^*} = \frac{\operatorname{erfc}\left(\frac{y}{2\sqrt{D_T\frac{x}{u}}}\right) + \operatorname{erfc}\left(\frac{a-y}{2\sqrt{D_T\frac{x}{u}}}\right)}{1 + \operatorname{erfc}\left(\frac{a}{2\sqrt{D_T\frac{x}{u}}}\right)}. \tag{12}$$

In Eq. 12, the sum in the numerator approximates the sidewall contribution, whereas the denominator normalizes the sum such that boundary conditions at both side walls are satisfied.

The major difference between this method and that of Coelho and Guedes de Carvalho[22] is that in their 3-D experimental method, the dissolving cylinder was placed along the axis of the packed bed, and the magnitudes of D_T were estimated based on the mass transfer rates between the soluble cylinder and the fluid flowing parallel to it.

System setup

The characteristics of the setups that were used for the numerical simulations are shown in Table 1 and Table 2. The flow was laminar (i.e., $Re < 100$ [42]). The standard porosity of the system (ε) was 0.35; however, in order to study the effects of porosity on the dispersion coefficients, porosities of 0.25, 0.30, and 0.40 were also used in some setups. When the system was not packed with isometric particles ($d = 12$ mm), the diameters of the particles that were used in these simulations ranged from 8 to 16 mm, 6 to 18 mm, and 4 to 20 mm. Variations of particle-size distribution were performed to investigate its effects on the dispersion coefficients. In order to study the effects of packing structure on the dispersion coefficients, randomly packed systems were compared to piecewise-regularly packed systems (as in polycrystalline).

Results and Discussion

Transient and steady-state numerical simulations were performed with the 2-D porous-medium model in order to calculate D_L and D_T, respectively. For very low fluid velocities ($u \to 0$), dispersion is dominated by molecular diffusion, wherein the following condition is valid[45]

$$\frac{D_L}{D_m} = \frac{D_T}{D_m} = \frac{1}{\tau}, \tag{13}$$

where τ is a tortuosity factor. This tortuosity factor is different than the purely geometrical tortuosity, as the former is the square value of the latter.[46] The cases for low velocities are exemplified in Figure 3a and 3c for the longitudinal and transverse dispersion simulations, respectively. Increasing the velocity by two-orders of magnitude results in very different concentration distributions (see Figure 3b and 3d).

As indicated in Figure 3b, the concentration front is far from being a straight line in the direction perpendicular to the primary flow direction. This is due to the natural dispersion that occurs in a random system of particles, as previously described.

The estimation of D_L

Concentration profiles can be derived from the transient longitudinal dispersion simulations, as exemplified in Figure 4 for numerical simulation B4. By fitting Eq. 7 to these concentration distributions (solid lines), the values of

Table 2. Characteristics of Setups used for the Transverse Dispersion Simulations

Case	ε	Particle diameter [mm]	System size [m^2]	τ	D_T/D_m at $Pe_m = 0.2$	D_T/D_m at $Pe_m = 2.0$	D_T/D_m at $Pe_m = 20$
I1–6	0.35	12	1.0 × 1.0	1.47	0.74 ± 0.04	1.43 ± 0.25	10.4 ± 2.7
J*	0.35	12	1.0 × 1.0	1.25	0.80	1.00	4.16
K1–4	0.35	6–18	1.0 × 1.0	1.46	0.75 ± 0.02	1.85 ± 0.28	13.7 ± 2.6
L1–4	0.25	8–16	1.0 × 1.0	1.88	0.61 ± 0.03	1.45 ± 0.27	10.5 ± 2.4
M1–6	0.35	12	0.5 × 0.5	1.49	0.67 ± 0.03	1.60 ± 0.60	12.0 ± 6.0

*Packing is piecewise regular as in polycrystalline.
The D_T/D_m values are nondimensional transverse dispersion coefficients. The values behind "±" are standard deviations. Cases marked with 1–4 or 1–6 consist of four or six simulations, respectively, with the same setup but with different random positions of particles in the system. ε is the porosity and τ is the tortuosity factor.

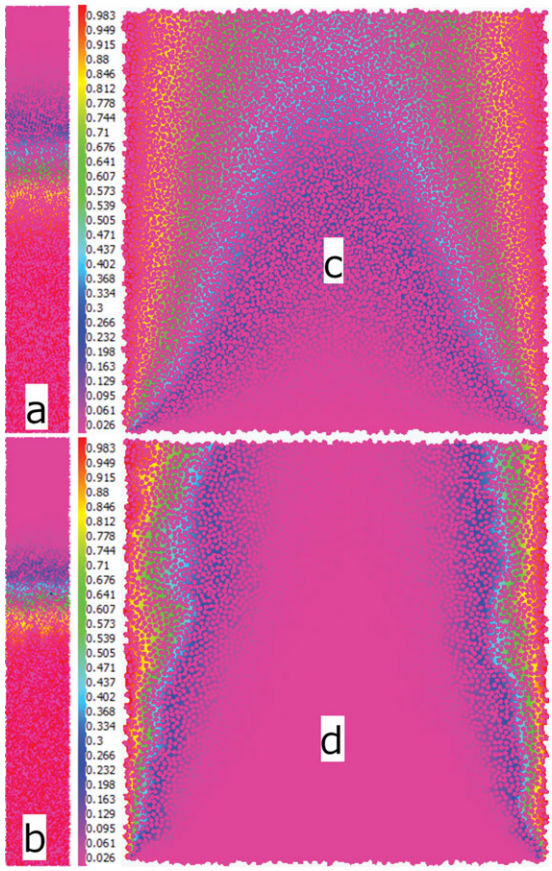

Figure 3. Concentration distributions in the calculation of D_L (snapshots): (a) $Pe_m = 0.2$ and $\varepsilon = 0.3$ (simulation A), (b) $Pe_m = 20$ and $\varepsilon = 0.4$ (simulation C), and concentration distributions in the calculation of D_T, (c) $Pe_m = 0.3$, and (d) $Pe_m = 30$.

[Color figure can be viewed in the online issue, which is available at wileyonlinelibrary.com.]

D_L/D_m were obtained (shown beside each respective curve). Note that the concentration may vary at any cross-section normal to the x-axis, as indicated by the error bars in Figure 4, which denote the standard deviations. In this context, the standard deviation is an important variable characterizing the unevenness of the flow front that strongly affects the apparent nonlocal dispersion. Equation 7 was simultaneously fitted to the concentration distribution curves during each transient longitudinal dispersion simulations. Using such a procedure, the values of D_L/D_m can be plotted as a function of time for each simulation. Figure 5 represents the cases for the numerical simulations A, B1, B2, C, F, and H1 for some different Pe_m.

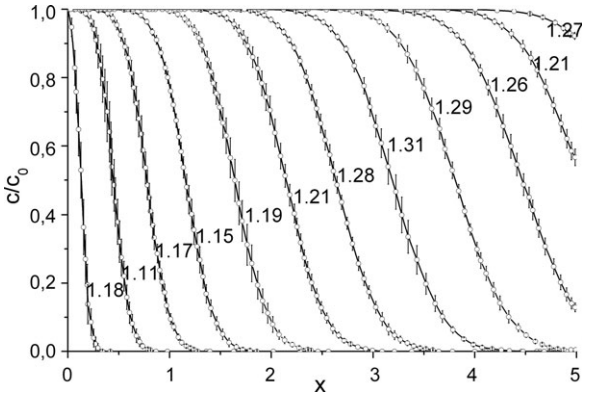

Figure 4. Flow-averaged (o) concentration profiles at various times vs. distance in the bed for a system of size 5.0 × 0.5 m^2, numerical simulation B4 and $Pe_m = 0.66666$.

The solid lines represent an approximation via the analytic formula of Eq. 7. The values of the estimated D_L/D_m are shown beside their respective curves. The error bars represent standard deviation of relative concentration in each cross-section perpendicular to the x-axis.

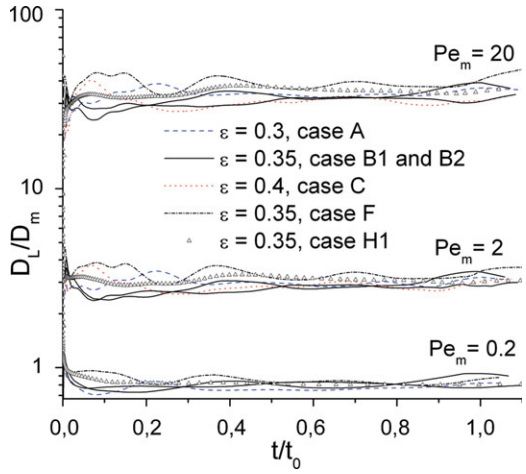

Figure 5. The development of the nondimensional longitudinal dispersion coefficients (obtained from flow-averaged concentration profiles) at different Pe_m vs. nondimensional time, numerical simulations A, B1, B2, C, F, and H1; $t_0 = L/u$.

[Color figure can be viewed in the online issue, which is available at wileyonlinelibrary.com.]

The 2-D system has to be fairly large to accurately calculate a final D_L. As can be seen in Figure 5, D_L needs some time, and, thus, also distance to stabilize, but toward the end of the 5 m long system the fluctuations cease, suggesting that a stable value of D_L is nearly reached. When the concentration front reaches the outlet, the fluctuations increase slightly due to the boundary condition at this end (i.e., $\partial c/\partial x = 0, x = L, t \geq 0$). However, it can be stated that the system is in most cases long enough to reduce variations of concentration at the cross-sections of the final parts of the system. The fluctuations are reduced when the width of the system is increased; see case H1 in Figure 5. However, an even larger system is required for unevenly-sized particles as for case F.

The initial peaks in Figure 5 are difficult to detect experimentally because they occur only in the first or possibly the second layer of the column, in which the thickness of a single layer corresponds to the average diameter of one particle d. Furthermore, the peak is not captured with the macroscopic advection-dispersion equation, which predicts a very small initial spreading. The spreading distance in this equation (i.e., $\sqrt{D_L t}$) is initially close to zero whereas in reality the minimum spreading distance is always greater than d. Thus, when applying a very short t in a discrete equation $d = \sqrt{D_L t}$, D_L must be very large to fulfill this equality, which is unrealistic. If t is long enough such that $d < \sqrt{D_L t}$, then the macroscopic equation is applicable.

The approximate solution to Eq. 1, given by Eq. 7, and the exact solution obtained with the CFITM code[44] were

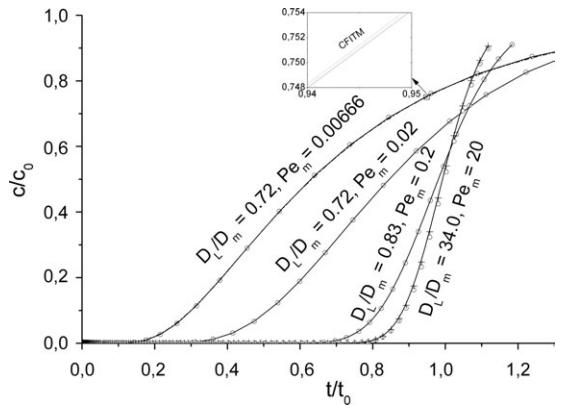

Figure 6. Flow-averaged (○) concentration effluent curves for a system of size 5.0 × 0.5 m², numerical simulation B1, vs. nondimensional time at various Pe_m.

The solid lines represent approximations via the analytical formula Eq. 7. The volume-averaged (+) concentration effluent curve is shown as an example for $Pe_m = 20$. The box to the top right shows an expanded section of the fitted effluent curve (dashed-dotted curve) via the CFITM code for $Pe_m = 0.00666$.

used to fit the effluent curves for one numerical simulation at low Pe_m (i.e., $Pe_m < 0.2$) with the purpose of comparing the two approaches. When one of the conditions in Eq. 8 is satisfied, the CFITM code uses Eq. 7, in order to fit the effluent curves. In this study, only at $Pe_m < 0.2$ conditions in Eq. 8 are not satisfied. Therefore, the CFITM code used the infinite series solution to Eq. 1 in order to fit the numerical simulation effluent curves for $Pe_m < 0.2$. The difference between the fitting that was obtained by the CFITM code and Eq. 7 was marginal; the fitted breakthrough curves almost coincide with one another (see Figure 6). Comparison between the estimated D_L by the CFITM code and Eq. 7 showed that the latter estimated D_L with three significant digits accuracy. Therefore, the estimated values of D_L that were used to calculate Pe_L were obtained by fitting Eq. 7 to the flow-averaged concentration effluent curves (see Figure 6). From this figure, it is also clear that flow-averaged and volume-averaged concentration profiles coincide.

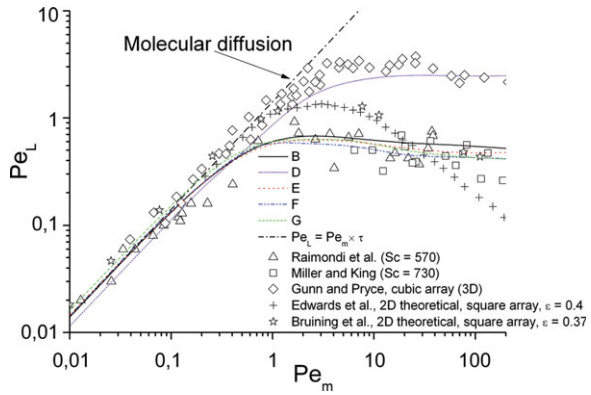

Figure 7. Calculated Pe_L in a packed-bed model from numerical simulations B, D, E, F, and G in comparison to 2-D theoretical data from Edwards et al.[47] and Bruining et al.[48] and 3-D experimental data from Raimondi et al.[33] Miller and King,[49] and Gunn and Pryce.[50]

[Color figure can be viewed in the online issue, which is available at wileyonlinelibrary.com.]

Parameter study

Simulations were performed for the cases presented in Tables 1 and 2 and the calculated values of D_L and D_T are shown as Pe_L and Pe_T plots vs. Pe_m in Figures 7 and 8, respectively.

The Effects of Particle-Size Distribution. In the numerical simulations, four particle-size distributions were used: uniform-sized particles and the distributions described in the section system setup; it should be noted that $d = 12$ mm was used for calculations of Pe_L and Pe_T for all cases. At very low Pe_m (wherein the dispersion is governed by molecular diffusion), variation of particle-size distribution does not affect the dispersion coefficients (see differences, at $Pe_m < 1$, between simulations B, E, and F in Table 1, and those between I and K in Table 2). The reason is particle size does not affect the tortuosity;[39] thus, the effect of particle-size distribution on dispersion coefficients at very low Pe_m is marginal. For both longitudinal and transverse dispersion simulations, at $Pe_m > 1$, D_L and D_T increases as the particle-size distributions become wider. More specifically, in the case of longitudinal dispersion simulations, as the ratio of maximum to minimum particle diameters goes from a value of 1 (i.e., uniform-size particles) to 2, D_L increases by 10% (see the difference between simulations B and E in Table 1 and Figure 7 at $Pe_m > 1$). Likewise, increasing the ratio of particle diameters from 2 to 5 results in an increase of D_L by roughly 12% (see the difference between simulations E and F in Table 1 and Figure 7 at $Pe_m > 1$). For D_T the effect is even larger and the simulations yield a 31% increase when different-size particles were used instead of uniform-size particles (see the difference between simulations I and K in Table 2 and Figure 8 at $Pe_m > 1$). The increase of D_L as the particle-size distribution becomes wider is in agreement with other studies.[33–37] One possible explanation is that as the particle-size distributions become wider the flow front becomes more uneven, which in turn amplifies the dispersion. In the case of D_T, 2-D calculations by Eidsath et al.[34] showed a reduction of the transverse dispersion with increased distribution of particle diameters. Hence, the results of this study contradict those in Eidsath et al. This

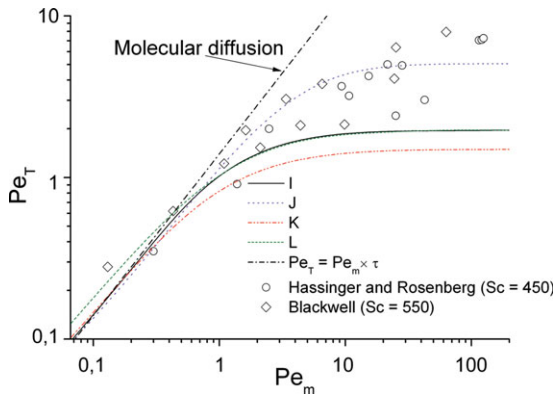

Figure 8. Calculated Pe_T in a packed-bed model from numerical simulations I, J, K, and L in comparison to 3-D experimental data from Hassinger and Rosenberg[51] and Blackwell.[52]

[Color figure can be viewed in the online issue, which is available at wileyonlinelibrary.com.]

might be traced to the spatially periodic porous-medium model that was used in Eidsath et al. The 3-D experiments of Han et al.[35] and Guedes de Carvalho and Delgado[38] showed that the transverse dispersion did not change at all with particle-size distribution. The difference between the 2-D results presented, herein, and 3-D experimental data obtained by Han et al. and Guedes de Carvalho and Delgado might be related to the 2-D approach that was used to calculate D_T; nevertheless, in 2-D, this result clearly supports the increase of D_T with increase of particle-size distributions.

The Effects of Packing Structure. For both longitudinal and transverse simulations, the differences between the obtained dispersion coefficients were significant between the randomly-packed systems and piecewise-regularly packed systems. For both longitudinal and transverse simulations, the tortuosity factor decreased when the system was packed piecewise regularly and thus D_L and D_T increased at very low Pe_m (see differences at $Pe_m < 1$ between simulations B and D in Table 1 and Figure 7, and between cases I and J in Table 2 and Figure 8). The reason is the flow path is less tortuous in the case of regular structure and thus the tortuosity factor decreases. At $Pe_m > 1$, the values of D_L and D_T were much lower in the case of piecewise-regularly packed systems compared to the systems that had been packed randomly (see differences at $Pe_m > 1$ between simulations B and D in Table 1 and Figure 7, and between cases I and J in Table 2 and Figure 8). The reason is the flow front in the regular case is almost flat and the additional dispersion associated with uneven flow front is relatively small; therefore, the ordered structure gives less dispersion at high Pe_m.

The Effects of Porosity. Decreasing the porosity of the porous medium increases the tortuosity factor,[39] and, thus, reduces the magnitudes of D_L and D_T for all cases studied at very low Pe_m (say, $Pe_m < 1$). Tables 1 and 2 provide comparison between the values of τ from simulations of I and K to L, C to B, B to A, and E to G. The explanation for this observation is that as the porosity decreases, the porous medium becomes more densely packed, which in turn increases the sinuosity of the flow path, resulting in increased tortuosity factor.

At higher Pe_m ($Pe_m > 1$), the dispersion is nearly independent of the porosity. However, the various dispersion mechanisms at high Pe_m make it not possible to easily determine the effect of porosity on the dispersion coefficients.

The Effects of Column Length. A comparison of longitudinal dispersion simulations H to E shows that by increasing the length of the setup from $L = 2.5$ m to $L = 5$ m, the magnitude of D_L increased by roughly 3.5% at $Pe_m > 1$ (see Table 1 for comparison between simulations H to E). This is expected since D_L increases as a function of the measurement scale; however, the statistical error needs to be reduced further to allow definitive conclusions. Comparison between transverse simulations M and I shows the importance of the size of the system, as the statistical variation increases substantially for a smaller system such as case M with half the length and width of system I (see Table 2 for comparison between simulations M and I as well as their respective standard deviations).

Comparisons of calculated Pe_L, Pe_T, and τ, to experimental and theoretical data

The derived D_L and D_T (shown as Pe_L and Pe_T vs. Pe_m, respectively) are here validated with previous theoretical calculations,[47,48] and experimental data[33,49–52] from the literature for the high values of Sc and $Pe_m \leq 200$ (which is the case in this study, see Figures 7 and 8). There is a lack of reference experimental data for 2-D systems so the numerical results are presented together with 2-D theoretical calculations and 3-D experimental data for dispersion in packed beds. In 3-D the fluid obviously has an additional dimension to use but previous research has shown that regarding permeability several trends can be captured with a 2-D approach despite the actual levels differ from a complete 3-D modeling.[53] The obtained values of τ from this 2-D packed bed of circular particles were compared to those of 3-D packed beds of spheres, because the reported values of τ in the literature are restricted to beds of spheres.[39,54] An exception is the study of England and Gunn[55] who reported a value of $\tau = 1.93$ for solid cylinders. However, the way that the particles in their experiment were positioned in the packed bed (with sharp edges) is completely different than this study (see Figure 6 in England and Gunn[55]). Moreover, as stated later in Gunn,[56] packing of solid cylinders in that previous study (England and Gunn[55]) was noticeably poor. Thus, this 2-D numerical-derived τ for circular particles cannot be compared to $\tau = 1.93$ for solid cylinders. Additionally, Gunn[56] stated that there exist considerable experimental difficulties in the measurement of dispersion in liquid phase at small Re, as the usual method to achieve small Re is to reduce the size of the particle, and the small particles become prone to the disturbance by the flow of liquid.

At very low values of Pe_m, both longitudinal and transverse dispersions are governed by molecular diffusion, and the values of Pe_L and Pe_T are the same (i.e., $Pe_L = Pe_T = Pe_m \times \tau$, see Figures 7 and 8). The estimated values of Pe_L and Pe_T at very low Pe_m, are in agreement with those of 2-D theoretical and 3-D experimental data (see Figures 7 and 8). The molecular diffusion line (shown in Figures 7 and 8) was calculated assuming a tortuosity factor, $\tau = 1.4$, as suggested by Gunn,[56] which has been established for spherical particles.

In this study, the values of τ for the piecewise-regularly packed beds were 1.15 (longitudinal case D, Table 1), and 1.25 (transverse case J, Table 2). For randomly packed beds τ found to be in the range of 1.37–1.88 (Tables 1 and 2), which was the decreasing function of porosity.[39] The obtained values of τ for the randomly packed beds were in the range reported in the literature for spheres (for an overview, see Lanfrey et al.[39]).

As can further be seen from Figure 7, the longitudinal dispersion numerical results are in excellent agreement with experimental data. Guedes de Carvalho and Delgado[37] showed that for $Sc > 750$, the dependence of Pe_L on Sc is slight, and in the range $100 < Pe_m < 5{,}000$, values of Pe_L are very nearly constant, for each value of Sc. Unfortunately, their experimental data did not cover the values of Pe_L for lower values of Pe_m (i.e., $Pe_m < 100$) for $Sc = 1930$ or $Sc = 1358$. Nevertheless, their experimental result, that is, $Pe_L \approx 0.4$ for $Sc = 1930$ and $Sc = 1358$ is consistent with this numerical results for Pe_L at $Pe_m > 1$. As mentioned previously, the value of Sc is assumed to be very large in this study. The difference between the previous 2-D theoretical data[47,48] shown in Figure 7 and present 2-D data at $Pe_m > 0.2$ is perhaps because of the simple porous-medium model (spatially periodic array of cylinders) that was used in their calculations comparing to this randomly packed-bed model. The Pe_T that were obtained from numerical simulations were found to be lower than the experimental data at $Pe_m > 1$.

Based on comparison of the simulated dispersion coefficients that were obtained by this 2-D packed-bed model to

the 3-D experimental data, this 2-D approach to investigating the D_L in flow through packed beds for the high values of Sc may be interpreted as acceptable. The observed larger D_T for a high value of Pe_m that was obtained by this model may be explained by noting that the lateral fluid motion (which strongly affects transverse dispersion) in a 2-D porous medium is stronger than that in a 3-D case. Moreover, in a 3-D case, there always exist gaps (even for closely packed particles) through which the flow can pass. In a 2-D case, flow through closely packed particles is impossible, which means flow must pass around the closely packed part of the system. This, in turn, increases the magnitude of the transverse dispersion. Nevertheless, the 2-D longitudinal numerical data agreed with the 3-D experimental data. A more objective approach would be to compare this 2-D simulated data to 2-D experiment-derived Pe_L and Pe_T, such as the obtained Pe_L and Pe_T in a flow through a fibrous bed.

Conclusions

Longitudinal and transverse dispersion coefficients were calculated via a detailed simulation of mass transport in 2-D packed-bed models in the laminar flow regime. The 2-D packed-bed model was found to be capable of investigating the effects of particle-size distributions, packing structure, and porosity on the dispersion coefficients. A summary of the major findings is as follows:

- At $Pe_m > 1$, increasing the width of the particle-size distribution of the packed beds resulted in higher values of D_L and D_T. However, at $Pe_m < 1$, the effect of particle-size distribution was marginal.
- At $Pe_m > 1$, when the system was packed piecewise-regularly (as in polycrystalline), the obtained values of D_L and D_T were much lower compared to the identical system that had been packed randomly. However, at $Pe_m < 1$, the piecewise-regularly packed system showed slightly higher values of D_L and D_T.
- Decreasing the porosity of the random porous medium increased the tortuosity factor, τ, which in turn decreased the dispersion coefficients in the molecular diffusion regime (i.e., at very low Pe_m). The effect of porosity at high Pe_m was marginal.
- At low values of Pe_m, both longitudinal and transverse mixings were governed by molecular diffusion. These observations were obtained by comparing this numerical results at low Pe_m with previous 2-D theoretical and 3-D experimental data, as well as the molecular diffusion line (i.e., $Pe_L = Pe_T = Pe_m \times \tau$).
- The values of D_L that were obtained using the 2-D model agreed with the 3-D experimental data. Based on this comparison, it is not possible to draw major conclusions for the validity of this 2-D numerical data. Nevertheless, this 2-D approach to study the D_L in flow through packed beds for the high values of Sc can be considered to be acceptable.
- At high values of Pe_m, the values of the D_T that were obtained using this model were several-fold larger than the experimental values. This was possibly a result of the 2-D approach that was used to study transverse dispersion in a packed-bed model.

Acknowledgments

The financial support of the Swedish Research Council and Formas is gratefully acknowledged. We would like to acknowledge the helpful discussions with Prof. van Genuchten from the Dept. of Environmental Sciences, University of California, Riverside, CA. Special thanks to Prof. Delgado from the Departamento de Engenharia Química Faculdade de Engenharia da Universidade do Porto, Portugal, for providing us with his valuable collection of experimental data.

Notation

a = width of the packed bed
C = solute concentration
C_0 = initial concentration
C^* = equilibrium concentration of the solute, i.e., solubility
d = diameter of inert particles
d_{dis} = size of discrete element
D_L = longitudinal dispersion coefficient
D_m = molecular diffusion coefficient
D_T = transverse dispersion coefficient
L = length of the packed bed
t = time
u = interstitial velocity
U = superficial velocity
x = axial Cartesian co-ordinate
y = transverse Cartesian co-ordinate

Greek letters

ε = porosity
μ = liquid dynamic viscosity
ρ = liquid density
τ = tortuosity factor
ω = vorticity

Dimensionless groups

Pe_C = column Peclet number, $= uL/D_L$
Pe_{dis} = discretization Peclet number, $= ud_{dis}/D_m$
Pe_m = Peclet number based on the molecular diffusion coefficient, $= ud/D_m$
Pe_L = Peclet number based on the axial dispersion coefficient, $= ud/D_L$
Pe_T = Peclet number based on the transverse dispersion coefficient, $= ud/D_T$
Re = Reynolds number, $= \rho ud/\mu$
Sc = Schmidt number, $= \mu/\rho D_m$

Literature Cited

1. Yu B, Lee LJ, Cao H. Fractal characters of pore microstructures of textile fabrics. *Fractals*. 2001;9(2):155–163.
2. Movva S, Gang Z, Guerra D, Lee LJ. Effect of carbon nanofibers on mold filling in a vacuum assisted resin transfer molding system. *J Compos Mater*. 2009;43(6):611–620.
3. Nordlund M, Lundström TS, Frishfelds V, Jakovics A. Permeability network model for non-crimp fabrics. *Compos Part A Appl Sci Manufact*. 2006;37(6 SPEC. ISS.):826–835.
4. Nordlund M, Fernberg SP, Lundström TS. Particle deposition mechanisms during processing of advanced composite materials. *Compos Part A Appl Sci Manufact*. 2007;38(10):2182–2193.
5. Nordlund M, Lundström TS. Effect of multi-scale porosity in local permeability modelling of non-crimp fabrics. *Transp Porous Media*. 2008;73(1):109–124.
6. Masoodi R, Pillai KM. Darcy's law-based model for wicking in paper-like swelling porous media. *AIChE J*. 2010;56(9):2257–2267.
7. Masoodi R, Tan H, Pillai KM. Darcy's law-based numerical simulation for modeling 3D liquid absorption into porous wicks. *AIChE J*. 2011;57(5):1132–1143.
8. Lundström TS, Gustavsson LH, Jēkabsons N, Jakovics A. Wetting dynamics in multiscale porous media. Porous pore-doublet model, experiment and theory. *AIChE J*. 2008;54(2):372–380.
9. Frishfelds V, Lundström TS, Jakovics A. Lattice gas analysis of liquid front in non-crimp fabrics. *Trans Porous Media*. 2010;84(1): 75–93.
10. Slichter CS. Field measurement of the rate of movement of underground waters. US Geology Survey, Water Supply, Paper 140; 1905.
11. Taylor G. Dispersion of soluble matter in solvent flowing slowly through a tube. *Proc R Soc London Ser A Math Phys Sci*. 1953;219(1137):186–203.
12. Aris R. On the Dispersion of a solute in a fluid flowing through a tube. *Proc R Soc London Ser A Math Phys Sci*. 1956;235(1200):67–77.
13. Aris R. On the dispersion of a solute by diffusion, convection and exchange between phases. *Proc R Soc London Ser A Math Phys Sci*. 1959;252(1271):538–550.

14. Bear J. *Dynamics of Fluids in Porous Media*. New York, NY: Elsevier; 1972.
15. Scheidegger AE. *The Physics of Flow Through Porous Media*. 3d ed. Toronto, Canada: University of Toronto Press; 1974.
16. Dullien FAL. *Porous Media: Fluid Transport and Pore Structure*. San Diego, CA: Academic Press; 1979.
17. Saffman PG. A theory of dispersion in a porous medium. *J Fluid Mech*. 1959;6(3):321–349.
18. Saffman PG. Dispersion due to molecular diffusion and macroscopic mixing in flow through a network of capillaries. *J Fluid Mech*. 1960;7(2):194–208.
19. Koch DL, Brady JF. Dispersion in fixed beds. *J Fluid Mech*. 1985;154:399–427.
20. van Genuchten MTh, Alves WJ. Analytical Solutions of the One-Dimensional Convective-Dispersive Solute Transport Equation. *Technical Bulletin - US. Dept of Agriculture*; 1982:1661.
21. Robbins GA. Methods for determining transverse dispersion coefficients of porous media in laboratory column experiments. *Water Resour Res*. 1989;25(6):1249–1258.
22. Coelho MAN, Guedes de Carvalho JRF. Transverse dispersion in granular beds. Part 1. Mass transfer from a wall and the dispersion coefficient in packed beds. *Chem Eng Res Des*. 1988;66(2):165–177.
23. Delgado JMPQ. A critical review of dispersion in packed beds. *Heat Mass Transfer*. 2006;42(4):279–310.
24. Thompson KE, Fogler HS. Modeling flow in disordered packed beds from pore-scale fluid mechanics. *AIChE J*. 1997;43(6):1377–1389.
25. Augier F, Idoux F, Delenne JY. Numerical simulations of transfer and transport properties inside packed beds of spherical particles. *Chem Eng Sci*. 2010;65(3):1055–1064.
26. Freund Hr, Bauer Jr, Zeiser T, Emig G. Detailed simulation of transport processes in fixed-beds. *Ind Eng Chem Res*. 2005;44(16):6423–6434.
27. Magnico P. Hydrodynamic and transport properties of packed beds in small tube-to-sphere diameter ratio: pore scale simulation using an Eulerian and a Lagrangian approach. *Chem Eng Sci*. 2003;58(22):5005–5024.
28. Zeiser T, Lammers P, Klemm E, W. Li Y, Bernsdorf J, Brenner G. CFD-calculation of flow, dispersion and reaction in a catalyst filled tube by the lattice Boltzmann method. *Chem Eng Sci*. 2001;56(4):1697–1704.
29. Hellström JGI, Frishfelds V, Lundström TS. Mechanisms of flow-induced deformation of porous media. *J Fluid Mech*. 2010;664:220–237.
30. Ljung AL, Frishfelds V, Lundström TS, Marjavaara D. Discrete and continuous modelling of heat and mass transport in drying of a bed of iron ore pellets. *Drying Technol*. 2012;30(7):760–773.
31. Frishfelds V, Lundström TS. Modelling of particle deposition during impregnation of dual scale fabrics. *Plastics Rubber Compos*. 2011;40:65–69.
32. Frishfelds V, Hellström JGI, Lundström TS, Mattsson H. Fluid Flow Induced Internal Erosion within Porous Media: Modelling of the No Erosion Filter Test Experiment. *Transp Porous Media*. 2011:1–17.
33. Raimondi P, Gardner GHF, Petrick CB. *Effect of pore structure and molecular diffusion on the mixing of miscible liquids flowing in porous media*. AIChE-SPE Joint Symposium, San Francisco, CA; 1959.
34. Eidsath A, Carbonell RG, Whitaker S, Herrmann LR. Dispersion in pulsed systems-III. Comparison between theory and experiments for packed beds. *Chem Eng Sci*. 1983;38(11):1803–1816.
35. Han N-W, Bhakta J, Carbonell RG. Longitudinal and lateral dispersion in packed beds: Effect of column length and particle size distribution. *AIChE J*. 1985;31(2):277–288.
36. Wronski S, Molga E. Axial dispersion in packed beds: The effect of particle size non-uniformities. *Chem Eng Process*. 1987;22(3):123–135.
37. Guedes de Carvalho JRF, Delgado JMPQ. Effect of fluid properties on dispersion in flow through packed beds. *AIChE J*. 2003;49(8):1980–1985.
38. Guedes de Carvalho JRF, Delgado JMPQ. Lateral dispersion in liquid flow through packed beds at Pem < 1,400. *AIChE J*. 2000;46(5):1089–1095.
39. Lanfrey PY, Kuzeljevic ZV, Dudukovic MP. Tortuosity model for fixed beds randomly packed with identical particles. *Chem Eng Sci*. 2010;65(5):1891–1896.
40. Huang K, Toride N, van Genuchten MTh. Experimental investigation of solute transport in large, homogeneous and heterogeneous, saturated soil columns. *Transp Porous Media*. 1995;18(3):283–302.
41. Lundström TS, Gebart BR. Effect of perturbation of fibre architecture on permeability inside fibre tows. *J Compos Mater*. 1995;29(4):424–443.
42. Hellström JGI, Jonsson PJP, Lundström TS. Laminar and turbulent flow through an array of cylinders. *J Porous Media*. 2010;13(12):1073–1085.
43. Berlyand L, Panchenko A. Strong and weak blow-up of the viscous dissipation rates for concentrated suspensions. *J Fluid Mech*. 2007;578:1–34.
44. van Genuchten MTh. *Determining Transport Parameters from Solute Displacement Experiments*. US Salinity Laboratory, Riverside, CA.; 1980:118.
45. Koplik J, Redner S, Wilkinson D. Transport and dispersion in random networks with percolation disorder. *Phys Rev A*. 1988;37(7):2619–2636.
46. Gommes CJ, Bons A-J, Blacher S, Dunsmuir JH, Tsou AH. Practical methods for measuring the tortuosity of porous materials from binary or gray-tone tomographic reconstructions. *AIChE J*. 2009;55(8):2000–2012.
47. Edwards DA, Shapiro M, Brenner H, Shapira M. Dispersion of inert solutes in spatially periodic, two-dimensional model porous media. *Trans Porous Media*. 1991;6(4):337–358.
48. Bruining H, Darwish M, Rijnks A. Computation of the longitudinal and transverse dispersion coefficient in an adsorbing porous medium using homogenization. *Trans Porous Media*. 2012;91(3):833–859.
49. Miller SF, King CJ. Axial dispersion in liquid flow through packed beds. *AIChE J*. 1966;12(4):767–773.
50. Gunn DJ, Pryce C. Dispersion in packed beds. *Trans Inst Chem Eng*. 1969;47:341–350.
51. Hassinger R, von Rosenberg D. A mathematical and experimental examination of transverse dispersion coefficients. *Old SPE J*. 1968;8(2):195–204.
52. Blackwell R. Laboratory studies of microscopic dispersion phenomena. *Old SPE J*. 1962;2(1):1–8.
53. Lundström TS, Frishfelds V, Jakovics A. A statistical approach to permeability of clustered fibre reinforcements. *J Compos Mater*. 2004;38(13):1137–1149.
54. Mota M, Teixeira J, Bowen WR, Yelshin A. Binary spherical particle mixed beds: porosity and permeability relationship measurement. *Trans Filtrate Soc*. 2001;1(4):101–106.
55. England R, Gunn DJ. Dispersion, pressure drop, and chemical reaction in packed beds of cylindrical particles *Trans Inst Chem Eng*. 1970;48:265–275.
56. Gunn DJ. Axial and radial dispersion in fixed beds. *Chem Eng Sci*. 1987;42(2):363–373.

Manuscript received Oct. 13, 2011, revision received Apr. 8, 2012, and final revision received Jun. 4, 2012.